The Report Committee for Fei Tong
Certifies that this is the approved version of the following report:

Important Factors in Predicting Detection Probabilities for Radiation Portal Monitors

APPROVED BY
SUPERVISING COMMITTEE:

Supervisor:

Elmira Popova

David Morton

Important Factors in Predicting Detection Probabilities for Radiation Portal Monitors

by

Fei Tong, B.E.

Report

Presented to the Faculty of the Graduate School of

The University of Texas at Austin

in Partial Fulfillment

of the Requirements

for the Degree of

Master of Science in Engineering

The University of Texas at Austin

May 2010

Acknowledgements

I would like to first thank my advisor, Dr. Elmira Popova, for her supervision, guidance and patience throughout the course of this work. I would then like to thank Gregory Thoreson and Dr. Erich Schneider for collaboration and running simulations for this study. I also thank Dr. David Morton for his serious review and critical suggestions of this report. My thanks also go to Jessica WebsterLove, Yufen Shao, and Jing Zan for their helpful comments and discussions on writing a good quality report. Finally, this report is dedicated to my husband, my parents and my parents-in-law for their love, support, and encouragement.

Abstract

Important Factors in Predicting Detection Probabilities for Radiation Portal Monitors

Fei Tong, M.S.E.

The University of Texas at Austin, 2010

Supervisor: Elmira Popova

This report analyzes the impact of some important factors on the prediction of detection probabilities for radiation portal monitors (RPMs). The application of innovative detection technology to improve operational sensitivity of RPMs has received increasing attention in recent decades. In particular, two alarm algorithms, *gross count* and *energy windowing*, have been developed to try to distinguish between special nuclear material (SNM) and naturally occurring radioactive material (NORM). However, the use of the two detection strategies is quite limited due to a very large number of unpredictable threat scenarios.

We address this problem by implementing a new Monte Carlo radiation transport simulation approach to model a large set of threat scenarios with predefined conditions.

In this report, our attention is focused on the effect of two important factors on the detected energy spectra in RPMs, the mass of individual nuclear isotopes and the thickness of shielding materials. To study the relationship between these factors and the resulting spectra, we apply several advanced statistical regression models for different types of data, including a multinomial logit model, an ordinal logit model, and a curvilinear regression model.

By utilizing our new simulation technique together with these sophisticated regression models, we achieve a better understanding of the system response under various conditions. We find that the different masses of the isotopes change the isotopes' effect on the energy spectra. In analyzing the joint impact of isotopes' mass and shielding thickness, we obtain a nonlinear relation between the two factors and the gross count of gamma photons in the energy spectrum.

Table of Contents

List of Tables

List of Figures

1 INTRODUCTION

The deployment of radiation portal monitors (RPMs) has been considered an essential element for interdicting smuggled nuclear materials and improving the nation's security. The goal is to capture any suspect vehicles or people by surveying all vehicles/cargos entering ports of entry, while maintaining a fast throughput of commerce. As a result, the operational sensitivity of RPMs to certain threats of interest is critical to this application.

While the current RPMs have greatly reduced potential threats from outside, they are approaching the limits of passive detection technology, which is lacking in its ability to discriminate between special nuclear material (SNM) and naturally occurring radioactive material (NORM). This inefficiency results in frequent innocent alarms caused by NORM, an important factor for radiation screening at border crossings. Therefore, many studies have been conducted to attack this problem, including the introduction of energy windowing methods for radiation spectrum characterization of certain threat sources. However, the real problem is complicated by a variety of factors, which leads to difficulty in predicting detection probabilities for RPMs. This report aims to investigate the effect of some key factors on the system response through the employment of Monte Carlo radiation transport simulations and statistical regression models.

2 RADIATION PORTAL MONITORING SYSTEM

2.1 Introduction

RPMs are designed for scanning cargo containers or vehicles to detect threat materials of concern, such as nuclear weapons or special nuclear materials. Since early this century, RPMs have been, and are being, widely employed at U.S. ports of entry for the purpose of interdicting smuggled nuclear material and thereby enhancing the safety of the nation. Any vehicles or people trying to pass through the ports of entry are required to move through these RPMs, where a primary radiation screening is applied to scan all of them. The goal of primary radiation screening is to catch any suspicious vehicles or containers that might contain some radioactive material, while rapidly releasing the majority of commerce vehicles. For those suspicious vehicles which trigger radiation alarms in the primary screening, a secondary screening then follows to investigate them in more depth to identify any real threat objects.

RPMs are composed of multi-layered radiation detectors. Figure 2.1 shows a typical RPM system with four layered panels, two on top and two on bottom. Inside these panels are plastic scintillator materials used for gamma-ray detection. Since radioactive materials always emit various kinds of radiation and high-energy gamma radiation can be easily detected by plastic scintillators at a distance, the vast majority of currently deployed RPMs are plastic scintillator-based. Polyvinyl toluene (PVT), a cost-effective plastic scintillator material efficient in detecting gamma radiation, is the most commonly used for this application. We will from now on use PVT to refer to general plastic scintillator materials.

Figure 2.1: A typical RPM system for cargo screening[1]

(Reprinted with permission from Elsevier)

PVT has the ability to absorb energy from incident gamma rays, and then generate light that is subsequently collected and recorded as an energy spectrum of the original gamma rays. As the truck transporting nuclear material passes through a PVT-based RPM, the gamma rays generated by these threat materials can be quickly detected by the system to trigger a radiation alarm as a sign for secondary screening. Nonetheless, the response of a PVT-based RPM depends on a variety of factors. The light collection efficiency may change with the size and type of scintillator material. Also, the efficiency of translating scintillation light to recordable electronic signal is subject to environmental temperature. More importantly, the total energy absorbed by PVT is not precisely equal to the original energy of incident gamma rays. Furthermore, the absorbed energy is not

concentrated in discernable full-energy peaks, but is spread over a broad energy range, typically from a few kilo-electron volts (KeV) to several million electron volts (MeV) depending on the type of radiation source. Therefore, detailed isotopic identification of different radiation sources is almost never achievable in a traditional PVT-based RPM system. In general, the relationship between the original incident energy, the energy deposited in PVT, and the energy recorded in spectrum is highly complicated by many non-linear factors, not only the ones mentioned above, but also others such as the position and geometry of the detector system. Due to all these factors, the traditional RPMs provide only crude limited information on the spectral signature of a source of radiation, leading to a poor operational sensitivity of the system. Under these circumstances, it is critical to deepen our knowledge of the abnormal radiation signature from threat materials in order to develop effective detection strategies for smuggled nuclear material.

Although loss of information is inevitable in the application of PVT-based RPMs, the energy spectrum from a plastic scintillator material does to a large extent depend on the incident gamma radiation, and hence provides valuable information on the signature of the original radiation source. For example, in a 4-panel RPM system, we are able to compute total number of counts of incident gamma photons over the whole energy range, by averaging the gross counts from each of the four panels. This averaged gross count has been widely utilized as a key measure of original gamma-ray energy, with the ability of differentiating between low- and high-energy radiation sources.

2.2 "Nuisance" or "Innocent" Alarms

In addition to nuclear material, there are many other naturally-occuring materials that can produce radiation. Natural background radiation is one type of radiation

constantly present everywhere in the environment. It occurs naturally in the air, water, soil, plants, rocks, and even inside the human body. Moreover, most man-made building materials and medical products (e.g., ceramic glazed materials, polishing compounds and abrasives, and medical radionuclides) incorporate some sources which are of course non-harmful but can emit radioactive isotopes. Accordingly, the level of background radiation varies largely depending on location, weather and human activities.

The existence of natural background radiation is a problem for nuclear material detection in that the primary source of radiation detected in RPMs is this type of radiation. In order to eliminate the effect of background radiation while examining a vehicle, it is necessary to continuously record the average background count rate when vehicles are not present in front of detectors. Once a vehicle arrives and passes through a detector at a certain speed, a new data set of radiation count rate can be obtained and compared with the most recent recorded background rate. By characterizing the difference between the data with and without vehicles, we can determine appropriate detection technology and alarm algorithms for our purpose.

However, the system does not always work as expected. Based on the alarm algorithm widely applied in current RPMs, radiation alarms are often triggered by non-threatening sources of radiation, primarily from those man-made naturally occurring radioactive material (NORM). Since these alarms arise from the presence of actual radioactive material, they are treated as real alarms, not the false alarms from a statistical point of view (Type I or Type II error in hypothesis test). For this reason, such an alarm is referred to as a “Nuisance” or “Innocent” alarm. As stated earlier all vehicles that trigger radiation alarms in the primary radiation screening are assumed to be suspicious and must proceed to secondary screening. Thus, frequent occurrence of nuisance alarms will

significantly increase the operational cost due to additional screening. Besides this, to stop and relocate a vehicle to another location for a secondary screening slows down the overall flow of commerce.

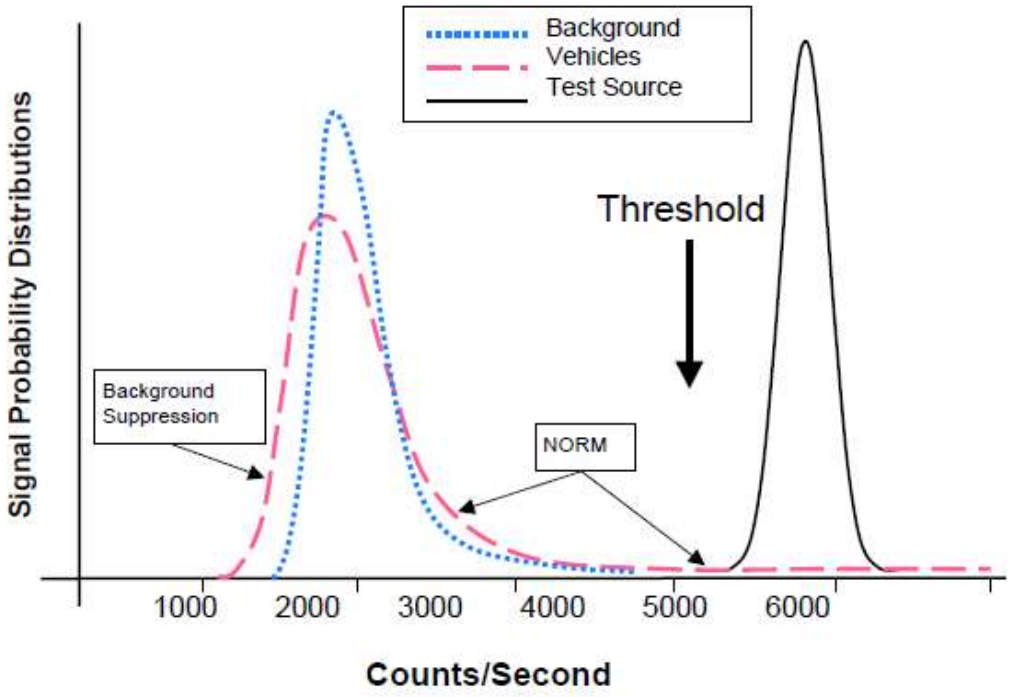

Figure 2.2: An example of gross-count rates of gamma photons detected in a RPM system[1]

(Reprinted with permission from Elsevier)

Figure 2.2 from Ely et al. [1] shows the normalized distributions of average gross-count rates of gamma photons from different radiation sources. The data displayed in the figure are obtained from a typical PVT-based RPM system with four panels. The dotted curve illustrates the distribution of natural background radiation collected prior to the

presence of vehicles. Note that the background counting rate is centered at 2000 counts-per-second (cps), but with a tail containing higher count rates, which can reach up to 3800 cps. This high-count-rate tail results from environmental changes surrounding the detectors. The dashed curve is the distribution of average gross-count rate when cargo vehicles are present. In comparison with the "Background" curve, we can see that this "Vehicles" curve is somewhat skewed to the left of "Background" and has a much longer tail in the range of high-count rate. This skewed distribution, present in all deployed RPM systems, is caused by a phenomenon known as "Shadow Shielding." As a cargo vehicle moves through the gamma-ray detectors, these detectors will be temporarily shielded by the cargo and the vehicle from the background radiation, resulting in a decreased number of gamma photon counts that can be detected in the system. The high-count-tail displayed in the "Vehicles" distribution is contributed by NORM cargo. The figure clearly shows that some NORM can produce very high levels of radiation (more than 6000 cps). The other distribution included in this figure is a simulated gross-count rate from an isolated test source, shown by the solid curve. Here the term "isolated" means that the radiation from this test source is collected without any shielding methods and is exempted from natural background radiation. Coincidently, the test source distribution overlaps with the high-count-tail of the cargo vehicles distribution (resulting from NORM). This fact indicates that if gross count is used as the only measure for nuclear material detection, then the appearance of NORM will almost always trigger an alarm in primary radiation screening. Even if this detection strategy were practical to capture SNM, it is not ideal simply because the alarms generated by NORM are all nuisance alarms, which will greatly reduce the overall operational sensitivity of the system and increase its operational cost.

2.3 Alarm Algorithms for Radiation Detection

A variety of alarm algorithms have been and are being studied to improve the operational sensitivity of RPMs to certain threat sources of interest. Gross count algorithm was the first approach introduced for this application, and is currently employed in all RPM systems. However, the inefficiency of the gross count algorithm in discriminating SNM from NORM limits its effectiveness as a radiation screening technology. The energy windowing algorithm is a more sophisticated approach designed to address this problem by reducing the frequent nuisance alarms.

2.3.1 GROSS COUNT ALGORITHM

The simplest and the most straightforward measure of a radiation signature is the total number of counts of gamma photons in a detector. The alarm is tripped if the detected gross count increases above some threshold. The threshold is set at different values in different locations, determined by many factors, such as natural background radiation, NORM cargo frequencies, and traffic flow rate constraints. In a traditional RPM system, a gross-count threshold is typically defined by the following equation:

$$T = N + K\sqrt{N}, \tag{2.1}$$

where T is the threshold count rate, N is the mean count rate from background radiation, $\sqrt{N}$ is the standard deviation of that background (which we assume is Poisson distributed), and K is a multiplier factor that determines the deviation of threshold count from the mean background count.

This equation demonstrates that the gross count threshold is based on the differentiation of test sources from background radiation, without considering NORM radiation, the major contributor of nuisance alarms. From Figure 2.2, we can clearly see

that the total counts originating from NORM may reach as high as, and even higher than the counts originating from the test threat source. As a result, the simple gross-count alarm algorithm is found to be unable to discriminate NORM from SNM in the primary screening of cargo vehicles.

2.3.2 ENERGY WINDOWING ALGORITHM

As discussed above, the gross count algorithm provides very little information on the energy of detected gamma photons and is ineffective in distinguishing different sources of radiation. To address this problem, the energy windowing algorithm has been developed by making use of the difference between the spectral signatures of NORM and of certain threat materials of interest. Figure 2.3 displays a result from Ely et al. [1], in which the energy spectra from two NORM sources (fertilizer and tile) and two man-made nuclear sources (plutonium and highly enriched uranium (HEU)) are compared to the energy spectrum from background radiation. As seen in Figure 2.3A, although both fertilizer and tile have higher intensity (number of gamma photons) than background radiation over the broad energy range, they actually share a similar shape of distribution with background. In contrast, nuclear sources display quite different shapes than background, as shown in Figure 2.3B, with much higher intensity in the low-energy part of the spectrum. This suggests that the spectral signatures of NORM and SNM are not the same, which offers an opportunity to distinguish one from the other.

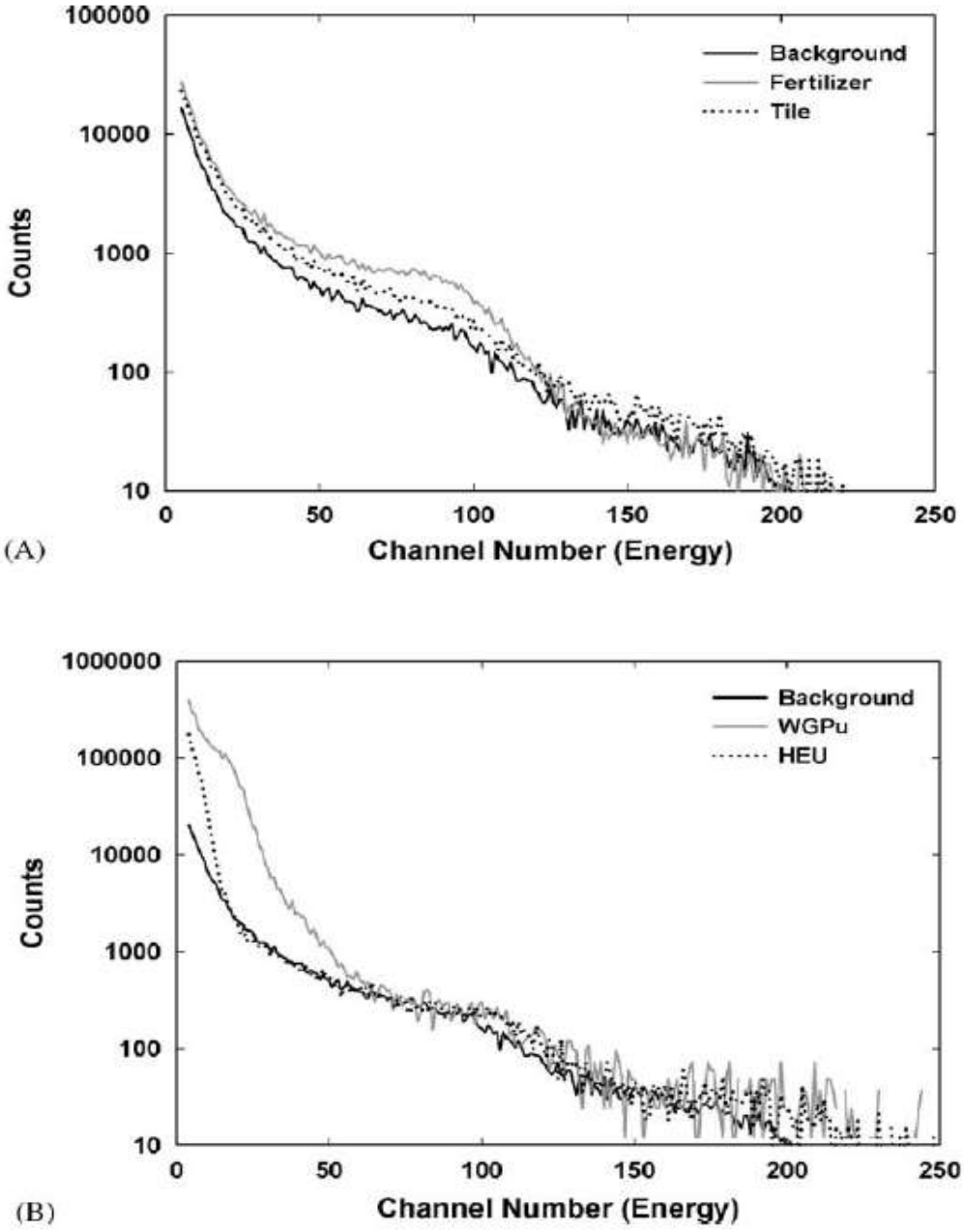

Figure 2.3: Energy spectra from PVT for (A) NORM (fertilizer and tile) and background, and (B) SNM (WGPu and HEU) and background.[1]

(Reprinted with permission from Elsevier)

An energy windowing algorithm aims to make use of the difference between SNM, NORM and background spectra by dividing the broad range of the energy spectrum into several non-overlapping "windows" or "bins", and quantifying the difference or similarity between the test signatures in these energy windows and the corresponding background signatures in the same windows. There are competing methods proposed for fully utilizing the information contained in these windows. Consider a n-window system ($n \gg 2$). One common method is to take the ratio of the gamma photon counts in each of the low-energy windows to the total counts in the remaining high-energy windows, then compare that ratio to the corresponding background ratio. This comparison can be expressed as

$$R_j = \frac{N_j}{\sum_{i=j+1}^{n} N_i} - \frac{N_{Bj}}{\sum_{i=j+1}^{n} N_{Bi}}, \tag{2.2}$$

where R_j refers to "Ratio j", N_j is the number of photon counts in the jth window of the test source spectrum, $\sum_{i=j+1}^{n} N_i$ is the combined counts from window $j+1$ to window n, N_{Bj} is the number of photon counts in the jth window of background spectrum, and $\sum_{i=j+1}^{n} N_{Bi}$ is the combined counts from window $j+1$ to window n. Because of the similarity of the shape of energy distributions in NORM and background, there should not be much difference between the ratio obtained from NORM and the ratio obtained from background (i.e., making R_j close to 0). In contrast, the gamma rays generated by SNM are primarily from the low-energy windows, resulting in a significantly different energy distribution than background, so distinct ratios are expected from SNM and background (i.e., R_j will be far away from 0).

Other methods may involve different combinations of windows, but generally they all show very similar results to the above method. In recent studies, such energy windowing algorithms have been shown to be very effective in discriminating between NORM and certain threat sources of interest and hence capable of reducing the NORM-caused nuisance alarms at RPMs. Furthermore, energy windowing can also be useful in other settings, such as in mitigating the impact of shadow shielding and in crude spectroscopy identification [2].

2.4 Radiation Transport Simulation

As discussed above, an energy windowing approach is theoretically efficient in discriminating NORM from SNM. However, it should be realized that the application of this approach is limited due to the huge number of possible sets of threat scenarios. The shape of the detected energy spectrum in a PVT detector is complicated by various types of nuclear isotopes, random combination of these isotopes, diverse shielding methods, and many other uncertain factors. Since such data are almost never available from the real commercial vehicles at RPMs, one common method is to use Monte Carlo radiation transport simulation as a system design tool for smuggled nuclear material interdiction applications.

2.4.1 THREAT SCENARIOS

We now describe how threat scenarios are defined and how simulation is used to estimate detection probabilities (DPs). Our description in this section relies heavily on Thoreson and Schneider [4]. A typical threat scenario is defined as a combination of various threat sources (e.g., plutonium, HEU, and their associated isotopes), the

surrounding environment (shielding, container, and cargo), detection technology, and an alarm algorithm. By simulating different scenarios, we can estimate the detection probability (DP) to determine the performance of different detection technologies and alarm algorithms. A good simulation approach is critical to developing the best detection strategy, especially when facing the computational burden of modeling large scenario sets. For this reason, a prevalent approach is to model a simplified version of the problem by selecting some typical scenarios as representative of the system. This approach does successfully reduce the computation time to a reasonable level. However, what it sacrifices is a loss of accuracy in the results. To overcome this obstacle while still maintaining an acceptable amount of computational effort, we adopt a new simulation approach in this study.

The new approach involves first, decomposition of a scenario into five independent submodels; second, parameterization of each submodel by major scenario variables; and third, simulation of each submodel independently within the entire scenario. The five submodels are: (1) threat source, (2) shielding, (3) host medium, (4) detector, and (5) environmental radiation. For threat source, we parameterize it using the mass, and assume the source is a solid sphere (the shape with the most conservative surface-area-to-volume ratio). For shielding methods, a lead shell is assumed to surround the source sphere. The thickness of the lead shell is a major contributor for changes in detected energy spectrum from the test source. Host medium refers to the vehicle or container and the cargo where the threat source and its shielding hide. We restrict our attention to commercial truck-trailers, but consider three categories of cargo materials surrounding the source and shielding. The three cargo types are categorized according to their shielding effectiveness. In addition, the impact of cargo shielding is further

parameterized by the location of the threat source inside the cargo. The forth submodel is for the detector. We consider a PVT-based detector, which is parameterized by the thickness of the detector. The last submodel is designed to account for the effect of environmental radiation, also known as background radiation. The gamma radiation from soil and concrete is modeled in this study.

The five submodels are formulated with independent parameters and functions. After that, the next step is to perform independent simulation for each submodel. Finally, it is necessary to integrate the separate results from these submodels into a full scenario. The detailed parameterization techniques and integration methods are beyond the scope of this report and will not be covered here.

2.4.2 IMPLEMENTATION

The weapons-grade plutonium isotopes (^{236}Pu, ^{238}Pu, ^{239}Pu, ^{240}Pu, ^{241}Pu) and HEU isotopes (^{232}U, ^{234}U, ^{235}U, ^{236}U, ^{238}U) are considered in this framework. In order to sufficiently capture spectral information from threat scenarios, we divide the whole range of energy spectrum into fourteen energy windows. This 14-window structure is employed throughout the simulations.

In each simulation, a unique threat source is contained in a truck-trailer, surrounded by shielding material and cargo, and moved through a RPM in specified time intervals. The gamma radiation leaving this test source and all shielding is collected by PVT and then translated to energy spectrum with a known overall collection rate. The counts of gamma photons are summed in each energy window, and passed to an alarm algorithm, where a detection probability is calculated.

2.5 Our Objective

To develop an appropriate detection technology for RPM application, it is essential to deepen our understanding of the behavior of the system. In this report, our objective is to study the spectral signatures from those simulated threat scenarios, try to identify the underlying trends, and ultimately provide better prediction of system response. In order to achieve this goal, we will take advantage of some sophisticated statistical regression models and inferential techniques to provide high-quality solutions with more insights into the system.

3 GENERALIZED LOGIT MODELS

Generalized logit models are well-developed statistical methods for analyzing categorical data. They can be used to study the effects of a set of explanatory variables on a categorical response variable and predict the probability for each category of the response variable. In this study, we are concerned with a categorical response variable *count* (number of gamma photons) in each of the 14 energy windows, for which generalized logit models would be appropriate to choose for analysis. This section discusses the techniques for different types of generalized logit models as well as their applications.

3.1 Introduction

In categorical data analysis, binary logit models are designed for binary responses, response variables with only two categories. Generalized logit models are the extension of binary logit models to handle the problems involving response variables with more than two categories. Depending on the structure of the response categories, generalized logit models can be classified into two different types: multinomial logit models and ordinal logit models. Multinomial logit models are used for nominal response variables, which have no intrinsic ordering to the categories. In comparison, ordinal logit models are used for ordinal response variables, whose categories possess a natural ordering structure that may be utilized to produce more insight into the relationship between the explanatory and response variables. All these logit models allow multiple

explanatory variables either categorical or continuous, whereas there can be only a single categorical response variable.

3.2 Multinomial Logit Models

Suppose Y is the response variable with J categories $y_1, y_2, \cdots, y_J$, and $\boldsymbol{X} = (1, X_1, X_2, \cdots, X_k)$ is a vector of explanatory variables. In a multinomial logit model, we select a response category y_j as a *reference category*. The goal is to analyze the effect of $\boldsymbol{X}$ on the response of Y by comparing the number of occurrence of each response category with the number of occurrence of the reference category. For illustration, let's pick y_J , the last category, as the reference response. We define $p_j(\boldsymbol{x})$ as the probability of response $y_j, j = 1, 2, \cdots, J$, given the knowledge of $\boldsymbol{x} = (1, x_1, x_2, \cdots, x_k)$. The multinomial logit model is then given in the form of

$$\log\left(\frac{p_j(\boldsymbol{x})}{p_J(\boldsymbol{x})}\right) = \alpha_j + \boldsymbol{\beta_j'}\boldsymbol{x} = \alpha_j + \beta_{j1}x_1 + \beta_{j2}x_2 + \cdots + \beta_{jk}x_k,$$

$$j = 1, 2, \ldots, J-1. \qquad (3.1)$$

The term $\log\left(\frac{p_j(\boldsymbol{x})}{p_J(\boldsymbol{x})}\right)$ on the left-hand side of this equation is called the jth sample logit – the log odds of response y_j relative to the reference response y_J. On the right-hand side, α_j is a constant value associated with the jth logit. The set of parameters $\boldsymbol{\beta_j} = (\beta_{j1}, \ldots, \beta_{jk})$ is a vector of regression coefficients for the jth logit obtained through maximum likelihood estimation procedures. We can see that there are a total of $J-1$ logits in the model, one for each response category except the reference category y_J. Therefore, the whole model consists of $J-1$ sets of parameter estimates, one for each logit.

The predicted response probabilities are calculated from

$$p_j(\boldsymbol{x}) = \frac{\exp\left(\alpha_j + \boldsymbol{\beta_j'}\boldsymbol{x}\right)}{1 + \sum_{h=1}^{J-1} \exp(\alpha_h + \boldsymbol{\beta_h'}\boldsymbol{x})}, \quad j = 1, 2, \ldots, J-1. \tag{3.2}$$

$$p_j(\boldsymbol{x}) = \frac{1}{1 + \sum_{h=1}^{J-1} \exp(\alpha_h + \boldsymbol{\beta_h'}\boldsymbol{x})}, \quad j = J. \tag{3.3}$$

For illustration, suppose Y falls into three categories: y_1, y_2 and y_3, and X is a scalar explanatory variable to be considered. We choose y_3 as the reference category for comparison. This gives us the multinomial logit model

$$\log\left(\frac{p_1(x)}{p_3(x)}\right) = \alpha_1 + \beta_{11}x \tag{3.4}$$

$$\log\left(\frac{p_2(x)}{p_3(x)}\right) = \alpha_2 + \beta_{21}x\,. \tag{3.5}$$

The predicted probabilities for each response category are

$$p_1(x) = \frac{\exp(\alpha_1 + \beta_{11}x)}{1 + \exp(\alpha_1 + \beta_{11}x) + \exp(\alpha_2 + \beta_{21}x)} \tag{3.6}$$

$$p_2(x) = \frac{\exp(\alpha_2 + \beta_{21}x)}{1 + \exp(\alpha_1 + \beta_{11}x) + \exp(\alpha_2 + \beta_{21}x)} \tag{3.7}$$

$$p_3(x) = \frac{1}{1 + \exp(\alpha_1 + \beta_{11}x) + \exp(\alpha_2 + \beta_{21}x)}\,. \tag{3.8}$$

Now it is clear that these three probabilities all fall within the range of 0 to 1. More specifically, logistic regression fits the relationship between a scalar x and $p_j(x)$ with a special S-shaped curve which is monotonic increasing ($\beta > 0$) or decreasing ($\beta < 0$) within the range of 0 to 1, as shown in Figure 3.1. This fact is quite different from ordinary linear regression models, which have the major structural problem of risking the predicted probabilities falling outside the legitimate and meaningful range of 0 and 1, when dealing with categorical variables. As a result, logistic regression models are preferred to linear probability models for categorical data analysis.

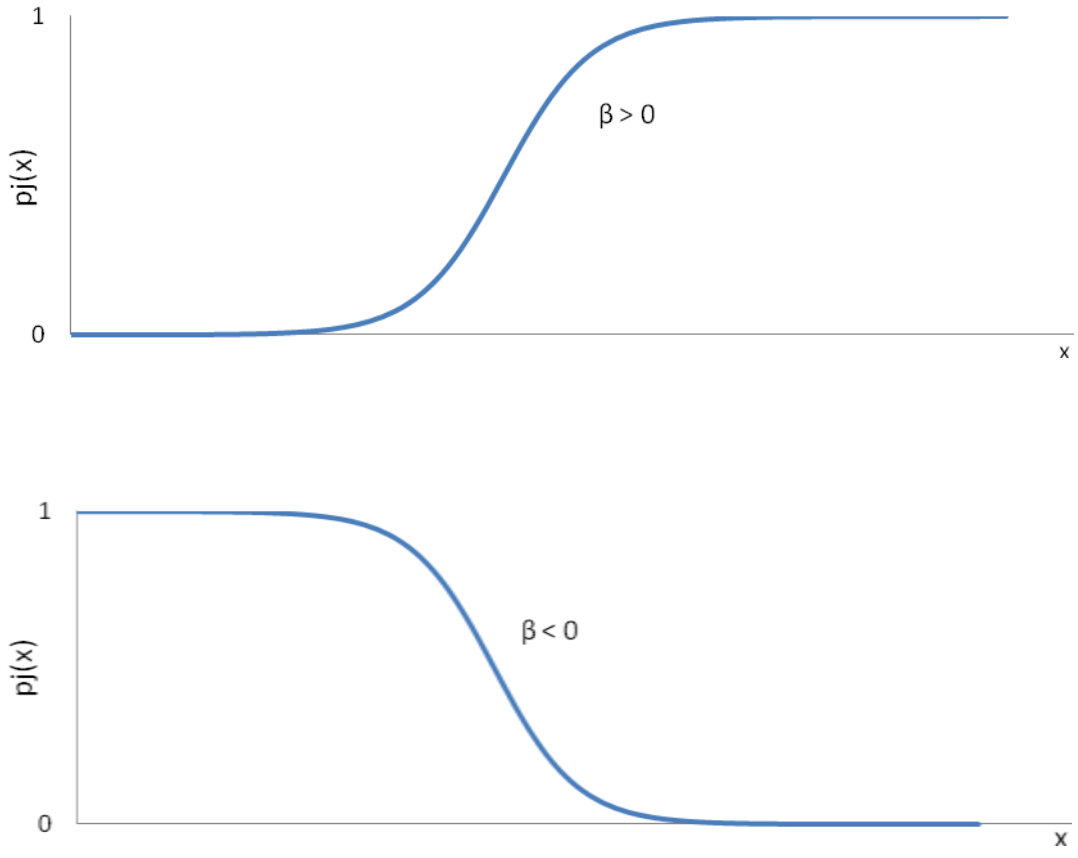

Figure 3.1: Logistic regression functions

3.3 Ordinal Logit Models

When the response categories of Y can be naturally ordered, say $y_1 < y_2 < \cdots < y_J$, one can take advantage of the ordering structure. The ordinal logit model is one type of logistic regression model that is widely used to take advantage of the ordering property of the response categories, which is done by forming logits of cumulative probabilities,

$$F_j(\boldsymbol{x}) = P\big(Y \le y_j \,\big|\boldsymbol{x}\big) = p_1(\boldsymbol{x}) + \cdots + p_j(\boldsymbol{x}), \qquad j = 1, 2, \cdots, J. \tag{3.9}$$

The *cumulative logits*, or *cumulative log odds*, are defined as

$$\text{logit}[F_j(\boldsymbol{x})] = \log\left(\frac{F_j(\boldsymbol{x})}{1 - F_j(\boldsymbol{x})}\right) = \log\left(\frac{p_1(\boldsymbol{x}) + \cdots + p_j(\boldsymbol{x})}{p_{j+1}(\boldsymbol{x}) + \cdots + p_J(\boldsymbol{x})}\right),$$
$$j = 1, 2, \ldots, J-1. \tag{3.10}$$

The ordinal logit model then refers to

$$\text{logit}[F_j(\boldsymbol{x})] = \alpha_j + \boldsymbol{\beta}'\boldsymbol{x} = \alpha_j + \beta_1 x_1 + \beta_2 x_2 + \cdots + \beta_k x_k,$$
$$j = 1, 2, \ldots, J-1. \tag{3.11}$$

For the J-category response variable, the whole model comprises $J-1$ cumulative logits. Each cumulative logit uses information from all J response categories. One important assumption inside the model is that the effect of each explanatory variable is the same on these cumulative logits, regardless the value of j. This means the coefficient associated with each x-variable, which is β_1 through β_k,

remains unchanged for all $J-1$ cumulative logit functions in the model. Under this assumption, it satisfies

$$\text{logit}[F_j(\boldsymbol{x_1})] - \text{logit}[F_j(\boldsymbol{x_2})] = \log\left(\frac{P(Y \le y_j \,|\boldsymbol{x_1}\,)/P(Y > y_j \,|\boldsymbol{x_1}\,)}{P(Y \le y_j \,|\boldsymbol{x_2}\,)/P(Y > y_j \,|\boldsymbol{x_2}\,)}\right)$$
$$= \boldsymbol{\beta}'(\boldsymbol{x_1} - \boldsymbol{x_2}). \qquad (3.12)$$

The term $\frac{P(Y\le y_j \,|\boldsymbol{x_1}\,)/P(Y>y_j \,|\boldsymbol{x_1}\,)}{P(Y\le y_j \,|\boldsymbol{x_2}\,)/P(Y>y_j \,|\boldsymbol{x_2}\,)}$ in this expression is called the *odds ratio* of cumulative probabilities for response category y_j, where the value of explanatory variable vector has changed from $\boldsymbol{x_1}$ to $\boldsymbol{x_2}$. As we can see, the log of the odds ratio is proportional to the difference between the two vectors of explanatory variables. Because of this property, the ordinal logit model (3.11) is also called a proportional odds model.

The predicted probabilities of each response category can be recovered by

$$p_j(\boldsymbol{x}) = P(Y \le y_j \,|\boldsymbol{x}\,) - P(Y \le y_{j-1} \,|\boldsymbol{x}\,) \qquad (3.13)$$

3.4 Comparison between multinomial logit and ordinal logit models

By comparing regression model (3.1) with model (3.11), we can identify two major differences between multinomial logit models and ordinal logit models. First, instead of choosing a reference category for comparison introduced in a multinomial logit model, the ordinal logit model makes use of the ordering structure of the response categories by comparing the cumulative probability of the lower categories with the probability of all higher categories. The cumulative logit for a response category y_j is the log odds of $P(Y \le y_j \,|\boldsymbol{x}\,)$ versus $P(Y > y_j \,|\boldsymbol{x}\,)$ given the presence of $\boldsymbol{x} = (1, x_1, x_2, \cdots, x_k)$. Therefore, all the J categories of response are considered in the cumulative logit. This is true for all the $J-1$ cumulative logits in the model. We also

know these cumulative logits are increasing in j, since they are increasing functions of $F_j(\boldsymbol{x})$, which is nondecreasing in j for fixed $\boldsymbol{x}$.

Second, multinomial logit models allow the effects of explanatory variables on different logits to be different and return a unique set of parameter estimates for each logit, which is $\boldsymbol{\beta}_j = (\beta_{j1}, \dots, \beta_{jk})$ for each response category j except the reference category. While on the other hand, ordinal logit models assume all explanatory variables have the same effect across different cumulative logits, resulting in a constant coefficient β_i associated with explanatory variable X_i, $i = 1, 2, \dots, k$, for all the $J-1$ cumulative logits. This is the so-called *proportional odds assumption* or *parallel regression assumption*. However, notice that even though the coefficient for each X remains the same, the proportional odds model does allow different intercepts across different cumulative logits. That is, we allow a unique α_j, $j = 1, 2, \dots, J-1$, for each of the cumulative log odds. For both multinomial logit and ordinal logit models, the unknown regression coefficients β_i's are all obtained by maximum likelihood estimation methods.

3.5 Model Selection and Evaluation

So far, we have introduced the techniques for analyzing the relationship between explanatory variables and a response variable in multinomial logit models and ordinal logit models. Two questions that remain are: (1) Which model should be selected in what conditions? (2) How can we evaluate and compare different fitted models?

3.5.1 PROPORTIONAL ODDS ASSUMPTION TEST

When there is an ordering structure in the categories of the response variable, an ordinal logit model is logically preferred to a multinomial logit model, as the information

included in the intrinsic ordering property can be helpful to make the model more parsimonious and hence may produce more accurate predicted probabilities and estimated expected frequencies. However, one should be always careful with the proportional odds assumption underlying the ordinal logit model, which states that the effect of an explanatory variable is constant across different cumulative logits. In other words, the regression functions are assumed to be parallel on the logit scale, with only distinct intercepts. This assumption simplifies the model on the one hand while imposing the restriction of proportionality on the other hand. It is not uncommon for a model not to satisfy the proportional odds assumption. If this is the case, an ordinal logit model is considered invalid, and we must switch to other alternative models (e.g., a multinomial logit model) to describe the relationship between each pair of response categories.

One advantage of using multinomial logistic regression is that there is no restriction on proportionality in that it assumes there is no order to the response categories. So the effect of an explanatory variable is expected to vary over different logits – log odds of the probability of each response versus the probability of reference response. However, if the response categories are truly ordered, applying multinomial logistic regression will result in the model losing the information contained in the structure of ordering.

As indicated above, the proportional odds assumption is a very important assumption for ordinal logit models. Therefore, it is necessary to test the validity of this assumption before applying the ordinal logit model to ordered categorical data. Some statistical software, such as SAS, can perform a score test for the proportional odds assumption. If we fail to reject the null hypothesis of having parallel regression equations, we conclude that the assumption holds and continue to use the ordinal logit

model for analysis. If we happen to reject the null hypothesis, we conclude that regression coefficients for explanatory variables are not equal across the cumulative logits and we fit a less restrictive model (i.e., in our case, multinomial logit model).

3.5.2 GOODNESS-OF-FIT TEST

For a fitted logistic regression model, we can test the overall fit of the model with several goodness-of-fit statistics. Two recommended tests for a generalized logit model are: a Pearson Chi-squared Test and a Deviance Log-likelihood Ratio Chi-squared Test. Both use chi-squared methods. That is, if the model fits the data well, these two goodness-of-fit statistics should be approximately distributed as chi-square with degrees of freedom equal to $(k-1) \times m - q$, where k is the number of levels or categories of the response variable, m is the number of explanatory variables, and q is the number of parameters required in the model. When the Pearson or the Deviance goodness-of-fit test is performed and the associated p-value is shown to be non-significant, we are confident that the model fits well with the data. If the p-value for the test is too small, it suggests that the current model doesn't fit with the data and we must try other alternative models for further study.

Usually the Pearson test and the Deviance Log-likelihood test will yield the same or very similar results for a fitted model, unless there is insufficient replication within the subgroups of the observations. In fact, to compute these goodness-of-fit test statistics, the original observations need to be first grouped into several subpopulations. If the data are too sparse and very few replications existed in the subgroups, the Pearson statistic and the Deviance statistic are no longer distributed as chi-square. In that case, there might be a

large difference between the Pearson statistic and the Deviance statistic, and the p-values for the two statistics are no longer valid and should be ignored.

4 COMPUTATIONAL RESUTLS

In this section, we perform regression analysis on two types of data sets: (1) a data set having one continuous explanatory variable and one categorical response variable; and (2) a data set having two continuous explanatory variables and one categorical response variable. All the data are generated from Monte Carlo radiation transport simulation, as discussed in Section 2.4. The analytical results are obtained with SAS/STAT software.

4.1 Test Data

Two groups of isotopes are examined in this study, weapons-grade plutonium isotopes (^{236}Pu, ^{238}Pu, ^{239}Pu, ^{240}Pu, ^{241}Pu) and HEU isotopes (^{233}U, ^{234}U, ^{235}U, ^{236}U, ^{238}U). Each group contains 5 different isotopes. We analyze the two groups separately, under the assumption that a typical threat source is comprised of a single group of isotopes.

4.2 Regression with One Explanatory Variable

The first type of data set considers only one explanatory variable. We are interested in the effect of the isotopes' mass on the resulting energy spectra. We study one isotope at a time. So for each group of isotopes, a total of five data sets are generated, one for each target isotope. In a data set, the simulation is repeated 100 times while varying the mass of one isotope and holding the mass of all other four isotopes constant.

The explanatory variable *mass* is the mass of the isotope of interest, which is varied from a decade below to a decade above its nominal mass inside an 8kg sphere. The resulting spectrum is divided into 14 energy windows/bins, from low- to high- energy. Our response variable *bin* is then created as an ordinal categorical variable with 14 categories representing the energy bins, denoted by $a1, a2, \cdots, a14$. The raw data is in the form of the number of gamma photon counts in each bin (the frequency of occurrence of each response category). We call this number *count*. Our goal is to build a logistic regression model to describe the relationship between the categorical response variable *bin* and the continuous explanatory variable *mass*. Since the 14 response categories have an ordering scale, we first try to fit an ordinal logit model. A score test is requested in SAS to test the validity of the proportional odds assumption. If the proportional odds assumption fails, we switch to fit a multinomial logit model. Table 4.1 shows the format of the data set used in this study.

In Table 4.2 and Table 4.3, we list the results of the proportional odds assumption tests for the group of plutonium isotopes and the group of HEU isotopes, respectively. The associated p-values for model Mass(^{238}Pu), model Mass(^{234}U), and model Mass(^{236}U) are greater than 0.05, indicating that the proportional odds assumption is valid in the three models. So we continue with the ordinal logit models to estimate these three models. In contrast, for the remaining 7 models whose p-values are less than 0.05, we have to reject the null hypothesis of proportional odds and switch to multinomial logit models.

Table 4.1: Data Format for One-predictor Model

Mass	Bin	Count
5.00E-09	a1	3.00E+02
5.00E-09	a2	7.52E+01
5.00E-09	a3	9.72E+01
5.00E-09	a4	1.47E+02
5.00E-09	a5	1.43E+02
5.00E-09	a6	1.67E+01
5.00E-09	a7	4.03E+01
5.00E-09	a8	3.83E+01
5.00E-09	a9	6.64E+01
5.00E-09	a10	1.75E+01
5.00E-09	a11	3.87E-01
5.00E-09	a12	1.11E-01
5.00E-09	a13	1.48E-01
5.00E-09	a14	1.05E-01
1.00E-08	a1	3.00E+02
1.00E-08	a2	7.52E+01
1.00E-08	a3	9.73E+01
1.00E-08	a4	1.47E+02
1.00E-08	a5	1.43E+02
1.00E-08	a6	1.67E+01
1.00E-08	a7	4.03E+01
1.00E-08	a8	3.83E+01
1.00E-08	a9	6.65E+01
1.00E-08	a10	1.76E+01
1.00E-08	a11	4.87E-01
1.00E-08	a12	2.21E-01
1.00E-08	a13	2.96E-01
1.00E-08	a14	2.11E-01

Table 4.2: Proportional Odds Assumption Test for Plutonium Isotopes

Explanatory Variable	Chi-squre	DF	Pr > ChiSq
Mass(^{236}Pu)	691.9255	12	< 0.001
Mass(^{238}Pu)	13.5081	12	0.3332
Mass(^{239}Pu)	423.569	12	< 0.0001
Mass(^{240}Pu)	88.5272	12	< 0.0001
Mass(^{241}Pu)	432.5814	12	< 0.0001

Table 4.3: Proportional Odds Assumption Test for HEU Isotopes

Explanatory Variable	Chi-squre	DF	Pr > ChiSq
Mass(^{232}U)	41.8795	12	< 0.0001
Mass(^{234}U)	6.2285	12	0.9041
Mass(^{235}U)	226.5845	12	< 0.0001
Mass(^{236}U)	0.7769	12	1
Mass(^{238}U)	1188.7261	12	< 0.0001

4.2. 1 ORDINAL LOGIT MODELS EVALUATION

The ordinal logit model employed for model Mass(^{238}Pu), Mass(^{234}U), and Mass(^{236}U) can be expressed in the form of

$$\log\left(\frac{\sum_{i=1}^{j} count_i}{\sum_{j+1}^{14} count_i}\right) = \alpha_j + \beta \cdot mass,$$

$$j = 1, 2, \dots, 13, \quad (4.1)$$

where $count_i$ refers to the count of photons in the ith energy bin. The explanatory variable *mass* stands for the mass of the isotope being varied, whose effect remains the same across all 13 cumulative logits, because of the proportional odds assumption.

Table 4.4 presents the main output from ordinal logistic regression analysis for isotope ^{238}Pu. The fact that the Deviance and Pearson Goodness-of-Fit statistics are not significant tells us our model fits the data well. Following are the results from three different tests of the overall model; they all indicate that the model is statistically significant. Next is the Analysis of Maximum Likelihood Estimates part, where we can see the coefficient of explanatory variable *mass*(^{238}Pu) is – 0.0434 with a small p-value of 0.0009. This means: (1) the variable *mass*(^{238}Pu) is statistically significant; (2) for a one unit increase in *mass*(^{238}Pu), there is an expected 0.0434 decrease in the cumulative log odds.

Table 4.5 shows the ordinal logistic regression output for isotope ^{234}U. According to the Deviance and Pearson Goodness-of-Fit statistics, our model fits the data well. However, the overall model is not statistically significant. This is so because the explanatory variable *mass*(^{234}U) with a p-value of 0.7656 is statistically insignificant.

Table 4.6 provides the output for isotope ^{236}U. Again, our model is good, but there is no statistically significant effect of *mass*(^{236}U) on the response variable *bin*.

Table 4.4: Ordinal Logistic Regression Output for ^{238}Pu

Deviance and Pearson Goodness-of-fit Statistics				
Criterion	Value	DF	Value/DF	Pr > ChiSq
Deviance	15.2002	1286	0.0118	1
Pearson	15.1827	1286	0.0118	1

Testing Global Null Hypothesis: β =0			
Test	Chi-Square	DF	Pr > ChiSq
Likelihood Ratio	11.0882	1	0.0009
Score	11.0901	1	0.0009
Wald	11.0885	1	0.0009

Analysis of Maximum Likelihood Estimates						
Parameter		DF	Estimate	Standard Error	Wald Chi-Square	Pr > ChiSq
Intercept	a1	1	-0.7484	0.0121	3803.8694	<.0001
Intercept	a2	1	-0.4033	0.012	1138.3346	<.0001
Intercept	a3	1	0.0106	0.0119	0.8013	0.3707
Intercept	a4	1	0.6431	0.0121	2842.4144	<.0001
Intercept	a5	1	1.4098	0.0128	12072.7477	<.0001
Intercept	a6	1	1.5213	0.013	13681.2449	<.0001
Intercept	a7	1	1.8386	0.0136	18220.6107	<.0001
Intercept	a8	1	2.2342	0.0147	23193.9512	<.0001
Intercept	a9	1	3.7039	0.0229	26224.9579	<.0001
Intercept	a10	1	5.5304	0.0511	11711.3582	<.0001
Intercept	a11	1	5.8191	0.0587	9829.9568	<.0001
Intercept	a12	1	6.2256	0.0715	7583.042	<.0001
Intercept	a13	1	6.9198	0.1005	4736.0898	<.0001
Mass(^{238}Pu)		1	-0.0434	0.013	11.0885	0.0009

Table 4.5: Ordinal Logistic Regression Output for ^{234}U

Deviance and Pearson Goodness-of-fit Statistics				
Criterion	Value	DF	Value/DF	Pr > ChiSq
Deviance	8.7508	1286	0.0068	1
Pearson	8.7409	1286	0.0068	1

Testing Global Null Hypothesis: β =0			
Test	Chi-Square	DF	Pr > ChiSq
Likelihood Ratio	0.0889	1	0.7656
Score	0.0889	1	0.7656
Wald	0.0889	1	0.7656

Analysis of Maximum Likelihood Estimates						
Parameter		DF	Estimate	Standard Error	Wald Chi-Square	Pr > ChiSq
Intercept	a1	1	-1.2193	0.0135	8169.4841	<.0001
Intercept	a2	1	-0.9371	0.0132	5070.7389	<.0001
Intercept	a3	1	-0.6537	0.0129	2555.7602	<.0001
Intercept	a4	1	-0.3566	0.0128	778.1759	<.0001
Intercept	a5	1	0.0108	0.0127	0.7231	0.3951
Intercept	a6	1	0.0723	0.0127	32.3019	<.0001
Intercept	a7	1	0.2473	0.0128	376.1219	<.0001
Intercept	a8	1	0.4345	0.0128	1149.8985	<.0001
Intercept	a9	1	0.7935	0.013	3706.9396	<.0001
Intercept	a10	1	1.113	0.0134	6945.0036	<.0001
Intercept	a11	1	1.4285	0.0138	10691.4332	<.0001
Intercept	a12	1	1.8316	0.0147	15618.662	<.0001
Intercept	a13	1	2.7768	0.0182	23242.9778	<.0001
Mass(^{234}U)		1	0.000011	0.000037	0.0889	0.7656

Table 4.6: Ordinal Logistic Regression Output for ^{236}U

Deviance and Pearson Goodness-of-fit Statistics				
Criterion	Value	DF	Value/DF	Pr > ChiSq
Deviance	1.5341	1286	0.0012	1
Pearson	1.5338	1286	0.0012	1

Testing Global Null Hypothesis: β =0			
Test	Chi-Square	DF	Pr > ChiSq
Likelihood Ratio	0	1	1
Score	0.0012	1	0.9722
Wald	0	1	1

Analysis of Maximum Likelihood Estimates						
Parameter		DF	Estimate	Standard Error	Wald Chi-Square	Pr > ChiSq
Intercept	a1	1	-1.2082	0.0136	7923.4564	<.0001
Intercept	a2	1	-0.927	0.0132	4901.9903	<.0001
Intercept	a3	1	-0.6458	0.013	2463.8462	<.0001
Intercept	a4	1	-0.3515	0.0129	746.7924	<.0001
Intercept	a5	1	0.0133	0.0128	1.0776	0.2992
Intercept	a6	1	0.0725	0.0128	32.0531	<.0001
Intercept	a7	1	0.2463	0.0128	368.4146	<.0001
Intercept	a8	1	0.4336	0.0129	1130.5105	<.0001
Intercept	a9	1	0.7913	0.0131	3638.6743	<.0001
Intercept	a10	1	1.1039	0.0134	6748.8686	<.0001
Intercept	a11	1	1.4115	0.0139	10330.1514	<.0001
Intercept	a12	1	1.8047	0.0147	15060.8913	<.0001
Intercept	a13	1	2.7442	0.0182	22694.9144	<.0001
Mass(^{236}U)		1	0	0.000088	0	1

4.2.2 MULTINOMIAL LOGIT MODELS EVALUATION

For the remaining 7 data sets, ^{236}Pu, ^{239}Pu, ^{240}Pu, ^{241}Pu, ^{233}U, ^{235}U, and ^{238}U, we can no longer fit ordinal logit models; instead we fit multinomial logit models to describe the relationship between the mass and the response variable. The lowest response category $bin = 'a1'$ is selected as the reference category for comparison. Then the multinomial logit model is defined as

$$\log\left(\frac{count_j}{count_1}\right) = \alpha_j + \beta_j \cdot mass\,,$$

$$j = 2, \dots, 14, \qquad (4.2)$$

where β_j is the regression parameter associated with *mass* for the jth logit.

From Table 4.7 to Table 4.13, we see non-significant goodness-of-fit statistics in all seven models. So we can say the overall model fit is good in every data set. We also know that these models are all statistically significant, because the Global Null Hypothesis Tests are significant. Next, we examine the effect of the variable *mass* on each logit. For each individual isotope, we can see its mass has a different impact among logits. Take ^{236}Pu for instance: the variable *mass*(^{236}Pu) is shown to be insignificant for the first 8 logits (from the 2nd to 9th bin), while it tends to be significant for the last 4 logits (from the 10th to 14th bin). However, as might be expected, this trend doesn't show in other isotopes, due to their distinct identities.

Table 4.7: Multinomial Logistic Regression Output for ^{236}Pu

Deviance and Pearson Goodness-of-fit Statistics				
Criterion	Value	DF	Value/DF	Pr > ChiSq
Deviance	152.8977	1274	0.12	1
Pearson	107.3553	1274	0.0843	1

Testing Global Null Hypothesis: β =0			
Test	Chi-Square	DF	Pr > ChiSq
Likelihood Ratio	820.9746	13	<.0001
Score	785.4517	13	<.0001
Wald	729.0961	13	<.0001

Analysis of Maximum Likelihood Estimates						
Parameter	Bin	DF	Estimate	Standard Error	Wald Chi-Square	Pr > ChiSq
Intercept	a2	1	-1.3872	0.0259	2868.2595	<.0001
Intercept	a3	1	-1.1285	0.0234	2321.2471	<.0001
Intercept	a4	1	-0.7121	0.0202	1242.019	<.0001
Intercept	a5	1	-0.7405	0.0204	1321.6931	<.0001
Intercept	a6	1	-2.9244	0.0509	3295.171	<.0001
Intercept	a7	1	-2.0171	0.0336	3607.5148	<.0001
Intercept	a8	1	-2.069	0.0343	3639.2407	<.0001
Intercept	a9	1	-1.5115	0.027	3136.6643	<.0001
Intercept	a10	1	-2.8509	0.0472	3649.8091	<.0001
Intercept	a11	1	-5.4868	0.1299	1783.4988	<.0001
Intercept	a12	1	-5.5135	0.1294	1816.7431	<.0001
Intercept	a13	1	-5.1366	0.1089	2226.1514	<.0001
Intercept	a14	1	-5.5454	0.1318	1771.3906	<.0001
Mass(^{236}Pu)	a2	1	1627.1	88428.3	0.0003	0.9853
Mass(^{236}Pu)	a3	1	152	79969.9	0	0.9985
Mass(^{236}Pu)	a4	1	-22308.5	69047.4	0.1044	0.7466
Mass(^{236}Pu)	a5	1	12122.6	69509.2	0.0304	0.8615
Mass(^{236}Pu)	a6	1	112559	172809	0.4243	0.5148
Mass(^{236}Pu)	a7	1	109977	113987	0.9309	0.3346
Mass(^{236}Pu)	a8	1	143069	116198	1.516	0.2182
Mass(^{236}Pu)	a9	1	175843	91345.3	3.7058	0.0542
Mass(^{236}Pu)	a10	1	782093	154296	25.6926	<.0001
Mass(^{236}Pu)	a11	1	4453106	358487	154.3049	<.0001
Mass(^{236}Pu)	a12	1	4661366	354346	173.0497	<.0001
Mass(^{236}Pu)	a13	1	4495903	300244	224.2255	<.0001
Mass(^{236}Pu)	a14	1	4630861	361278	164.3009	<.0001

Table 4.8: Multinomial Logistic Regression Output for ^{239}Pu

Deviance and Pearson Goodness-of-fit Statistics				
Criterion	Value	DF	Value/DF	Pr > ChiSq
Deviance	255.1691	1274	0.2003	1
Pearson	269.2406	1274	0.2113	1

Testing Global Null Hypothesis: β =0			
Test	Chi-Square	DF	Pr > ChiSq
Likelihood Ratio	617.2535	13	<.0001
Score	580.5066	13	<.0001
Wald	458.4945	13	<.0001

Analysis of Maximum Likelihood Estimates						
Parameter	Bin	DF	Estimate	Standard Error	Wald Chi-Square	Pr > ChiSq
Intercept	a2	1	-1.3928	0.0216	4152.5162	<.0001
Intercept	a3	1	-1.1326	0.0195	3368.651	<.0001
Intercept	a4	1	-0.7064	0.0167	1793.0572	<.0001
Intercept	a5	1	-0.7538	0.0171	1940.3335	<.0001
Intercept	a6	1	-2.9553	0.0447	4369.6918	<.0001
Intercept	a7	1	-2.0655	0.03	4730.4448	<.0001
Intercept	a8	1	-2.1232	0.0313	4599.4488	<.0001
Intercept	a9	1	-1.5692	0.0248	3994.0194	<.0001
Intercept	a10	1	-2.8871	0.0456	4008.8455	<.0001
Intercept	a11	1	-5.6722	0.2069	751.5814	<.0001
Intercept	a12	1	-4.4368	0.4005	122.7307	<.0001
Intercept	a13	1	-4.5919	0.2496	338.4993	<.0001
Intercept	a14	1	-4.566	0.4524	101.8514	<.0001
Mass(^{239}Pu)	a2	1	-1.82E-06	3.46E-06	0.2767	0.5988
Mass(^{239}Pu)	a3	1	-1.22E-06	3.12E-06	0.1528	0.6959
Mass(^{239}Pu)	a4	1	3.08E-06	2.66E-06	1.3396	0.2471
Mass(^{239}Pu)	a5	1	-6.02E-06	2.75E-06	4.8035	0.0284
Mass(^{239}Pu)	a6	1	-0.00002	7.29E-06	10.0095	0.0016
Mass(^{239}Pu)	a7	1	-0.00003	4.93E-06	47.8403	<.0001
Mass(^{239}Pu)	a8	1	-0.00005	5.19E-06	77.8036	<.0001
Mass(^{239}Pu)	a9	1	-0.00005	4.14E-06	175.8513	<.0001
Mass(^{239}Pu)	a10	1	-0.00006	7.67E-06	61.5784	<.0001
Mass(^{239}Pu)	a11	1	-0.00016	0.000039	17.7945	<.0001
Mass(^{239}Pu)	a12	1	-0.00212	0.000483	19.2279	<.0001
Mass(^{239}Pu)	a13	1	-0.00092	0.000123	55.6665	<.0001
Mass(^{239}Pu)	a14	1	-0.00231	0.000598	14.8987	0.0001

Table 4.9: Multinomial Logistic Regression Output for ^{240}Pu

Deviance and Pearson Goodness-of-fit Statistics				
Criterion	Value	DF	Value/DF	Pr > ChiSq
Deviance	55.59	1274	0.0436	1
Pearson	48.1704	1274	0.0378	1

Testing Global Null Hypothesis: β =0			
Test	Chi-Square	DF	Pr > ChiSq
Likelihood Ratio	109.2755	13	<.0001
Score	101.8058	13	<.0001
Wald	85.1093	13	<.0001

Analysis of Maximum Likelihood Estimates						
Parameter	Bin	DF	Estimate	Standard Error	Wald Chi-Square	Pr > ChiSq
Intercept	a2	1	-1.3872	0.0255	2959.975	<.0001
Intercept	a3	1	-1.1283	0.023	2396.779	<.0001
Intercept	a4	1	-0.7135	0.0198	1293.1056	<.0001
Intercept	a5	1	-0.7392	0.0201	1356.031	<.0001
Intercept	a6	1	-2.9128	0.0506	3309.3481	<.0001
Intercept	a7	1	-2.0044	0.0335	3584.4959	<.0001
Intercept	a8	1	-2.0537	0.0343	3579.233	<.0001
Intercept	a9	1	-1.4903	0.027	3039.4165	<.0001
Intercept	a10	1	-2.8137	0.0488	3318.0446	<.0001
Intercept	a11	1	-5.6858	0.202	792.2205	<.0001
Intercept	a12	1	-5.1926	0.2018	662.1873	<.0001
Intercept	a13	1	-5.6858	0.202	792.2205	<.0001
Intercept	a14	1	-4.989	0.2399	432.5089	<.0001
Mass(^{240}Pu)	a2	1	-0.00001	0.000071	0.0307	0.861
Mass(^{240}Pu)	a3	1	-8.57E-06	0.000064	0.0178	0.8938
Mass(^{240}Pu)	a4	1	0.000019	0.000055	0.1214	0.7275
Mass(^{240}Pu)	a5	1	-0.00004	0.000056	0.4361	0.509
Mass(^{240}Pu)	a6	1	-0.00012	0.000142	0.7291	0.3932
Mass(^{240}Pu)	a7	1	-0.00018	0.000094	3.8271	0.0504
Mass(^{240}Pu)	a8	1	-0.00023	0.000097	5.6278	0.0177
Mass(^{240}Pu)	a9	1	-0.00027	0.000076	12.7382	0.0004
Mass(^{240}Pu)	a10	1	-0.00027	0.000139	3.8025	0.0512
Mass(^{240}Pu)	a11	1	-0.0004	0.000579	0.4742	0.4911
Mass(^{240}Pu)	a12	1	-0.00395	0.000786	25.2398	<.0001
Mass(^{240}Pu)	a13	1	-0.0004	0.000579	0.4742	0.4911
Mass(^{240}Pu)	a14	1	-0.00891	0.00151	34.9959	<.0001

Table 4.10: Multinomial Logistic Regression Output for ^{241}Pu

Deviance and Pearson Goodness-of-fit Statistics				
Criterion	Value	DF	Value/DF	Pr > ChiSq
Deviance	231.2368	1274	0.1815	1
Pearson	223.6144	1274	0.1755	1

Testing Global Null Hypothesis: β =0			
Test	Chi-Square	DF	Pr > ChiSq
Likelihood Ratio	1096.9778	13	<.0001
Score	1087.1962	13	<.0001
Wald	1080.7167	13	<.0001

Analysis of Maximum Likelihood Estimates						
Parameter	Bin	DF	Estimate	Standard Error	Wald Chi-Square	Pr > ChiSq
Intercept	a2	1	-1.384	0.023	3629.0432	<.0001
Intercept	a3	1	-1.1263	0.0208	2920.52	<.0001
Intercept	a4	1	-0.7166	0.0183	1537.3576	<.0001
Intercept	a5	1	-0.7289	0.0179	1661.9229	<.0001
Intercept	a6	1	-2.8494	0.0413	4767.6901	<.0001
Intercept	a7	1	-1.926	0.0269	5114.9635	<.0001
Intercept	a8	1	-1.9506	0.0269	5253.8077	<.0001
Intercept	a9	1	-1.378	0.0212	4205.1087	<.0001
Intercept	a10	1	-2.7005	0.0374	5210.9699	<.0001
Intercept	a11	1	-5.6965	0.2083	747.9232	<.0001
Intercept	a12	1	-5.6307	0.2067	741.9977	<.0001
Intercept	a13	1	-5.6307	0.2067	741.9977	<.0001
Intercept	a14	1	-5.6307	0.2067	741.9977	<.0001
Mass(^{241}Pu)	a2	1	0.00192	0.000982	3.834	0.0502
Mass(^{241}Pu)	a3	1	0.00138	0.000893	2.374	0.1234
Mass(^{241}Pu)	a4	1	-0.00251	0.00079	10.1236	0.0015
Mass(^{241}Pu)	a5	1	0.00451	0.000761	35.0598	<.0001
Mass(^{241}Pu)	a6	1	0.0135	0.0017	62.3733	<.0001
Mass(^{241}Pu)	a7	1	0.0157	0.00111	199.7964	<.0001
Mass(^{241}Pu)	a8	1	0.0179	0.0011	264.0773	<.0001
Mass(^{241}Pu)	a9	1	0.019	0.000874	470.7683	<.0001
Mass(^{241}Pu)	a10	1	0.0188	0.00152	151.2219	<.0001
Mass(^{241}Pu)	a11	1	-0.0288	0.00996	8.3791	0.0038
Mass(^{241}Pu)	a12	1	-0.034	0.0101	11.3406	0.0008
Mass(^{241}Pu)	a13	1	-0.034	0.0101	11.3406	0.0008
Mass(^{241}Pu)	a14	1	-0.034	0.0101	11.3406	0.0008

Table 4.11: Multinomial Logistic Regression Output for ^{232}U

Deviance and Pearson Goodness-of-fit Statistics				
Criterion	Value	DF	Value/DF	Pr > ChiSq
Deviance	329.5251	1274	0.2587	1
Pearson	316.6174	1274	0.2485	1

Testing Global Null Hypothesis: β =0			
Test	Chi-Square	DF	Pr > ChiSq
Likelihood Ratio	354.6392	13	<.0001
Score	355.1191	13	<.0001
Wald	354.7416	13	<.0001

Analysis of Maximum Likelihood Estimates						
Parameter	Bin	DF	Estimate	Standard Error	Wald Chi-Square	Pr > ChiSq
Intercept	a2	1	-1.428	0.0257	3086.8637	<.0001
Intercept	a3	1	-1.2779	0.024	2842.8555	<.0001
Intercept	a4	1	-1.1267	0.0225	2501.6601	<.0001
Intercept	a5	1	-0.8388	0.0202	1722.1141	<.0001
Intercept	a6	1	-2.5925	0.0413	3942.4888	<.0001
Intercept	a7	1	-1.5575	0.0263	3500.6542	<.0001
Intercept	a8	1	-1.5224	0.026	3427.3398	<.0001
Intercept	a9	1	-0.9612	0.0212	2060.0407	<.0001
Intercept	a10	1	-1.2208	0.0233	2738.1782	<.0001
Intercept	a11	1	-1.3376	0.024	3105.865	<.0001
Intercept	a12	1	-1.2536	0.023	2969.7082	<.0001
Intercept	a13	1	-0.851	0.0199	1831.4867	<.0001
Intercept	a14	1	-1.1382	0.022	2688.4631	<.0001
Mass(^{232}U)	a2	1	3579.1	1540	5.4011	0.0201
Mass(^{232}U)	a3	1	6625.5	1430.4	21.4532	<.0001
Mass(^{232}U)	a4	1	8014.8	1342.6	35.6369	<.0001
Mass(^{232}U)	a5	1	9886.8	1203.2	67.5258	<.0001
Mass(^{232}U)	a6	1	11835.7	2439.9	23.5315	<.0001
Mass(^{232}U)	a7	1	11300.1	1560.3	52.4502	<.0001
Mass(^{232}U)	a8	1	10766.5	1542.6	48.7111	<.0001
Mass(^{232}U)	a9	1	8548.7	1262	45.8839	<.0001
Mass(^{232}U)	a10	1	8091.4	1390	33.8869	<.0001
Mass(^{232}U)	a11	1	12766	1421	80.7059	<.0001
Mass(^{232}U)	a12	1	15740.8	1357.6	134.4287	<.0001
Mass(^{232}U)	a13	1	16525.6	1175.3	197.7123	<.0001
Mass(^{232}U)	a14	1	16948.1	1294.6	171.3814	<.0001

Table 4.12: Multinomial Logistic Regression Output for ^{235}U

Deviance and Pearson Goodness-of-fit Statistics				
Criterion	Value	DF	Value/DF	Pr > ChiSq
Deviance	135.275	1274	0.1062	1
Pearson	133.9565	1274	0.1051	1

Testing Global Null Hypothesis: β =0			
Test	Chi-Square	DF	Pr > ChiSq
Likelihood Ratio	2932.7706	13	<.0001
Score	2897.0311	13	<.0001
Wald	2823.5311	13	<.0001

Analysis of Maximum Likelihood Estimates						
Parameter	Bin	DF	Estimate	Standard Error	Wald Chi-Square	Pr > ChiSq
Intercept	a2	1	-1.466	0.032	2094.7308	<.0001
Intercept	a3	1	-1.336	0.0316	1789.9621	<.0001
Intercept	a4	1	-1.1807	0.0307	1483.0722	<.0001
Intercept	a5	1	-0.8843	0.0281	988.6954	<.0001
Intercept	a6	1	-2.6494	0.062	1825.4378	<.0001
Intercept	a7	1	-1.6055	0.0383	1753.7473	<.0001
Intercept	a8	1	-1.5631	0.0376	1726.446	<.0001
Intercept	a9	1	-0.9782	0.0294	1104.3846	<.0001
Intercept	a10	1	-1.2254	0.0327	1404.1105	<.0001
Intercept	a11	1	-1.3975	0.0353	1569.8201	<.0001
Intercept	a12	1	-1.3614	0.0347	1534.9737	<.0001
Intercept	a13	1	-0.9731	0.0296	1077.8237	<.0001
Intercept	a14	1	-1.2651	0.0334	1437.0802	<.0001
Mass(^{235}U)	a2	1	-3.79E-06	7.23E-07	27.436	<.0001
Mass(^{235}U)	a3	1	-9.18E-06	7.43E-07	152.875	<.0001
Mass(^{235}U)	a4	1	-0.00001	7.49E-07	349.8839	<.0001
Mass(^{235}U)	a5	1	-0.00002	7.12E-07	684.5032	<.0001
Mass(^{235}U)	a6	1	-0.00002	1.65E-06	160.1595	<.0001
Mass(^{235}U)	a7	1	-0.00002	1.01E-06	420.7412	<.0001
Mass(^{235}U)	a8	1	-0.00002	9.86E-07	435.3431	<.0001
Mass(^{235}U)	a9	1	-0.00002	7.57E-07	704.3108	<.0001
Mass(^{235}U)	a10	1	-0.00002	8.54E-07	604.1263	<.0001
Mass(^{235}U)	a11	1	-0.00002	9.30E-07	536.491	<.0001
Mass(^{235}U)	a12	1	-0.00002	9.16E-07	555.6593	<.0001
Mass(^{235}U)	a13	1	-0.00002	7.73E-07	774.6518	<.0001
Mass(^{235}U)	a14	1	-0.00002	8.78E-07	604.7078	<.0001

Table 4.13: Multinomial Logistic Regression Output for ^{238}U

Deviance and Pearson Goodness-of-fit Statistics				
Criterion	Value	DF	Value/DF	Pr > ChiSq
Deviance	55.6663	1274	0.0437	1
Pearson	55.7329	1274	0.0437	1

Testing Global Null Hypothesis: β =0			
Test	Chi-Square	DF	Pr > ChiSq
Likelihood Ratio	1324.7186	13	<.0001
Score	1335.5082	13	<.0001
Wald	1314.6852	13	<.0001

Analysis of Maximum Likelihood Estimates						
Parameter	Bin	DF	Estimate	Standard Error	Wald Chi-Square	Pr > ChiSq
Intercept	a2	1	-1.4556	0.0312	2182.9639	<.0001
Intercept	a3	1	-1.3269	0.0293	2048.7862	<.0001
Intercept	a4	1	-1.1915	0.0276	1863.6717	<.0001
Intercept	a5	1	-0.9252	0.0252	1351.4875	<.0001
Intercept	a6	1	-2.7076	0.0536	2552.9083	<.0001
Intercept	a7	1	-1.6658	0.0338	2433.1243	<.0001
Intercept	a8	1	-1.6219	0.0329	2427.9423	<.0001
Intercept	a9	1	-1.0194	0.0256	1583.4564	<.0001
Intercept	a10	1	-1.2683	0.0279	2061.4455	<.0001
Intercept	a11	1	-1.4675	0.0318	2133.4052	<.0001
Intercept	a12	1	-1.4063	0.0333	1785.0508	<.0001
Intercept	a13	1	-0.991	0.029	1170.0628	<.0001
Intercept	a14	1	-1.2735	0.0328	1510.6145	<.0001
Mass(^{238}U)	a2	1	0.000016	7.02E-06	4.8753	0.0272
Mass(^{238}U)	a3	1	0.000028	6.57E-06	17.702	<.0001
Mass(^{238}U)	a4	1	0.000038	6.15E-06	38.7077	<.0001
Mass(^{238}U)	a5	1	0.000032	5.63E-06	32.2774	<.0001
Mass(^{238}U)	a6	1	0.000025	0.000012	4.3622	0.0367
Mass(^{238}U)	a7	1	0.000022	7.58E-06	8.61	0.0033
Mass(^{238}U)	a8	1	0.000031	7.35E-06	17.7534	<.0001
Mass(^{238}U)	a9	1	0.000053	5.68E-06	88.6131	<.0001
Mass(^{238}U)	a10	1	0.00006	6.16E-06	94.8765	<.0001
Mass(^{238}U)	a11	1	-2.64E-06	7.24E-06	0.1328	0.7155
Mass(^{238}U)	a12	1	-0.00009	8.04E-06	132.2966	<.0001
Mass(^{238}U)	a13	1	-0.00013	7.15E-06	328.7926	<.0001
Mass(^{238}U)	a14	1	-0.00014	8.21E-06	305.9372	<.0001

4.3 Regression with Two Explanatory Variables

Now we turn our attention to a model with two explanatory variables. In addition to the isotopes' mass, we are interested in the effect of shielding methods on the response energy spectrum. For the plutonium isotopes, we vary the total mass of the five isotopes from 100 grams to 6000 grams along with the lead shielding thickness from 0.1 to 5 cm. For the HEU isotopes, the total mass is varied from 100 grams to 20000 grams and the lead shielding thickness is from 0.1 to 2 cm. Here notice that although the total mass is varied, the proportions of the five isotopes in a group are kept unchanged. This means we assume the mass of all isotopes in a group is varied at the same rate. So the two explanatory variables in the model are: (1) *mass*, denoting total mass of a group of five isotopes; (2) *shield*, representing the lead shielding thickness. The simulation is run 10000 times for each group (100 changes of *mass* times 100 changes of *shield*). The data is formatted as shown in Table 4.14.

We attempt logistic regression for both plutonium and HEU isotopes, using the same procedures as we have done in the one-predictor case. Unfortunately, the results are not satisfactory. All the models show goodness-of-fit statistics being less than 0.0001, indicating a bad fit. Therefore, we conclude that logistic regression model is unachievable for the energy windowing analysis in the two-predictor case. Although the regression on separate energy windows does not work, we can still look at the overall spectral signature, by combining all the 14 energy windows to get the gross count of gamma photons.

Table 4.14: Data Format for Two-predictor Model

Mass	Shield	Bin	Count
1.00E+02	1.00E-01	a1	1.94E+02
1.00E+02	1.00E-01	a2	2.62E+01
1.00E+02	1.00E-01	a3	1.32E+01
1.00E+02	1.00E-01	a4	5.77E+00
1.00E+02	1.00E-01	a5	5.47E+00
1.00E+02	1.00E-01	a6	9.40E-01
1.00E+02	1.00E-01	a7	2.59E+00
1.00E+02	1.00E-01	a8	2.66E+00
1.00E+02	1.00E-01	a9	4.50E+00
1.00E+02	1.00E-01	a10	3.29E+00
1.00E+02	1.00E-01	a11	2.67E+00
1.00E+02	1.00E-01	a12	2.77E+00
1.00E+02	1.00E-01	a13	4.24E+00
1.00E+02	1.00E-01	a14	3.23E+00

4.3.1 CURVILINEAR REGRESSION FOR GROSS COUNT ANALYSIS

Now we have a new response variable *grosscount*, which is assumed to be continuous because the number of incident photons is very large; and two continuous explanatory variables: *mass* and *shield*. It is well known that, before any great effort is devoted to trying to fit an equation to a data set that has only a few continuous variables, it is always helpful to plot the data first and graphically observe the relationship between the variables. Here we investigate two scatter plots of *grosscount* versus *mass* and *grosscount* versus *shield*.

For plutonium isotopes, the scatter plot of *grosscount* versus *mass* is given in Figure 4.1. Data of this form appears to follow a power relationship

$$grosscount = \beta_0 (mass)^{\beta_1} . \tag{4.3}$$

Next, from Figure 4.2, we see that variables *grosscount* and *shield* seem to be related through an exponential function

$$grosscount = \beta_2 \exp(\beta_3 shield) . \tag{4.4}$$

By combining equation (4.3) and (4.4), a possible relation between the three variables can be determined in the form of

$$grosscount = \beta_0 (mass)^{\beta_1} \exp(\beta_3 shield) . \tag{4.5}$$

This is a nonlinear relationship, but is intrinsically linear. The reason is that after applying some simple mathematical transformations to the original nonlinear form, we

can in fact obtain a linear relation. Here we take the natural logarithm of both sides of the equation (4.5), which yields

$$\ln(grosscount) = \ln \beta_0 + \beta_1 \ln(mass) + \beta_3 shield$$

or, redefining β_0,

$$\ln(grosscount) = \beta_0 + \beta_1 \ln(mass) + \beta_3 shield\,. \qquad (4.6)$$

This new relation in equation (4.6) can be interpreted as

$$Y = \beta_0 + \beta_1 X_1 + \beta_2 X_2\ . \qquad (4.7)$$

Now, we can see the transformed variables are related by a simple linear equation. This fact tells us that if the response variable and the explanatory variables do have a nonlinear relationship indicated in equation (4.5), we can simply perform a linear regression analysis on the transformed data set, instead of a more complicated nonlinear regression on the original data set.

For HEU isotopes, it looks like the same relationship exists between *grosscount*, *mass* and *shield*, as shown in Figure 4.3 and 4.4. Therefore, the same curvilinear regression analysis can be performed on the HEU data set.

Having completed transformation on our original data sets, we achieve the curvilinear regression outputs from SAS/STAT. Table 4.15 presents the results for the plutonium data set. We first see that the overall model has a very large *F*-value of 182127 with a small *p*-value of < 0.0001. Thus we can confidently reject the null hypothesis and conclude that a significant relation exists between $\ln(grosscount)$, $\ln(mass)$, and

$shield$. In the next part, the multiple correlation coefficient squared (R-squared) is 0.97, which means that 97% of the total sum of squared errors (SST) is explained by the fitted model. This implies the model is a very good fit. Then we examine the individual parameters associated with each explanatory variable, and realize that all the coefficients have p-values less than 0.0001. This ensures that all the explanatory variables in the model are statistically significant. In view of the statistics shown in this table, we are confident this is a good regression for the plutonium data set. As a consequence, the fitted model is expressed by the following equation:

$$\ln(grosscount) = 5.14 + 2/3\ln(mass) - 1.49shield$$

or

$$grosscount = \exp(5.14)(mass)^{2/3}\exp(-1.49shield)\,. \qquad (4.8)$$

The HEU data set shows similar regression results, with an R-squared value of 0.9 and all the coefficients being statistically significant, as illustrated in Table 4.16. The fitted equation is

$$grosscount = \exp(1.28)(mass)^{2/3}\exp(-0.9shield)\,. \qquad (4.9)$$

4.3.2 FROM STATISTICS TO PHYSICS

We use statistical regression methods to obtain equations (4.8) and (4.9) for describing the relationship between operational factors and system response. The relation is justified not only from the statistical point of view, but also appears to be legitimate from the physical perspective of the system. First, the term $(mass)^{2/3}$ occurring in both equations is what we expect from the fact that the surface-to-volume ratio which governs

the radiation flux exiting the threat sources scales as $(mass)^{2/3}$. Second, the $\exp(5.14)(mass)^{2/3}$ term and $\exp(1.28)(mass)^{2/3}$ term give reasonable numbers of gross photon counts with no shielding. Third, the *shield* coefficients of –1.49 and –0.9 reflect the attenuation coefficients for the shield material (lead). For the sphere of plutonium isotopes, the lead shielding is varied from 0.1 to 5 cm. If we take the cross section for lead (in cm^{-1}), and weight it by the normalized spectrum leaving the plutonium sphere, we can get a weighted attenuation cross section very close to –1.5 cm^{-1}. For the sphere of HEU isotopes, we vary the lead shielding from 0.1 – 2 cm , and the resulting weighted attenuate is close to –0.9 cm^{-1}.

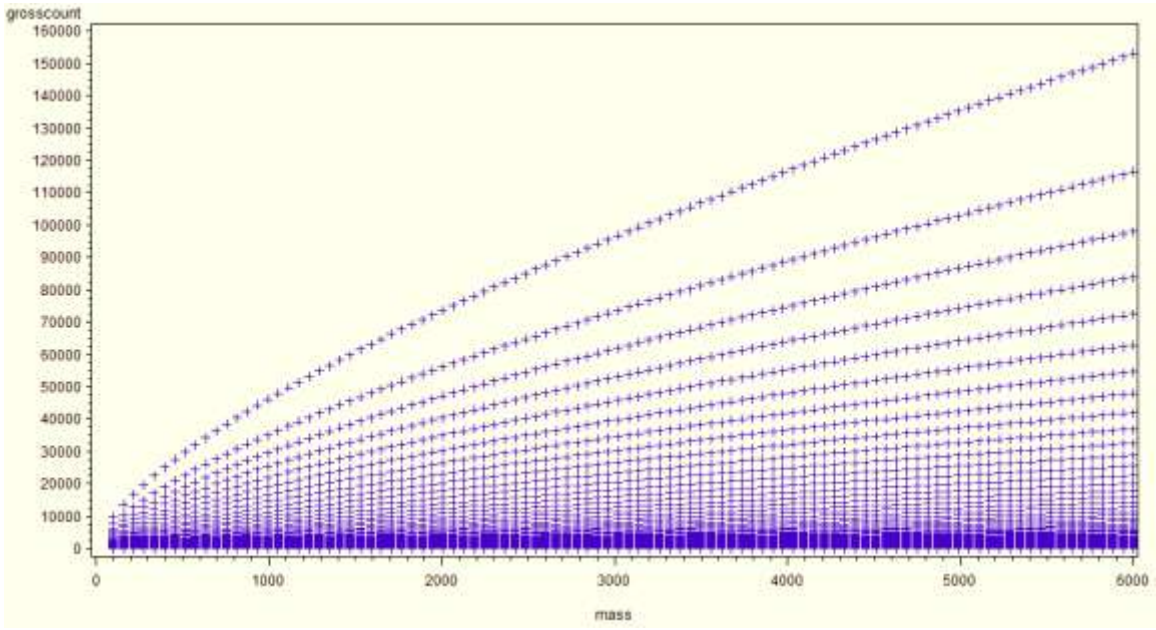

Figure 4.1: Scatter plot of *grosscount* versus *mass* for plutonium isotopes

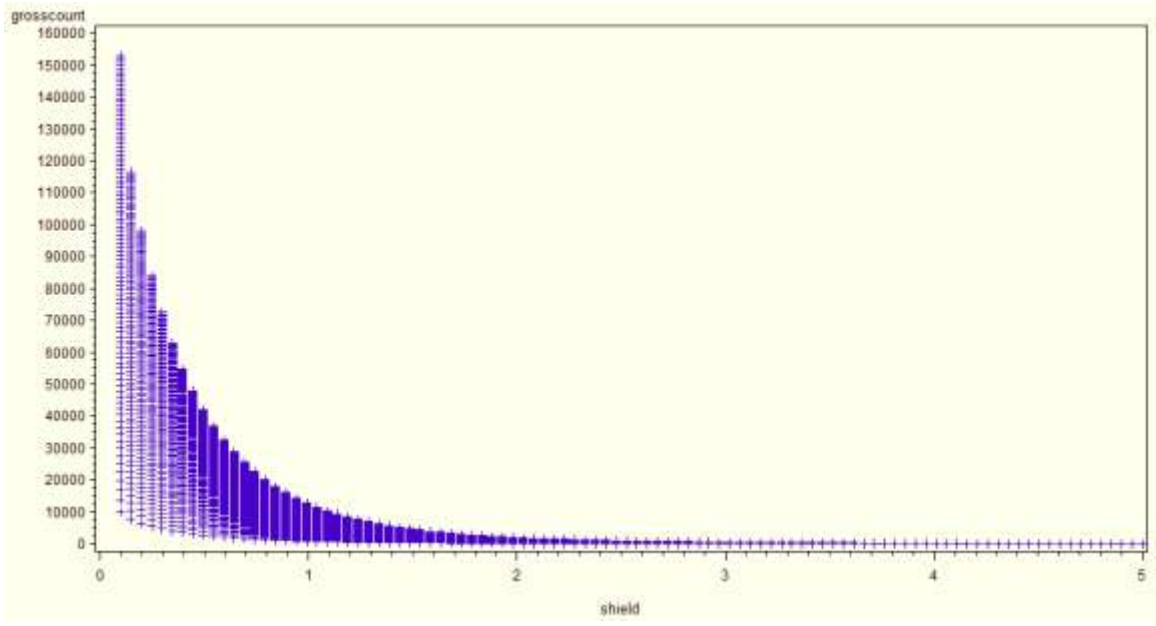

Figure 4.2: Scatter plot of *grosscount* versus *shield* for plutonium isotopes

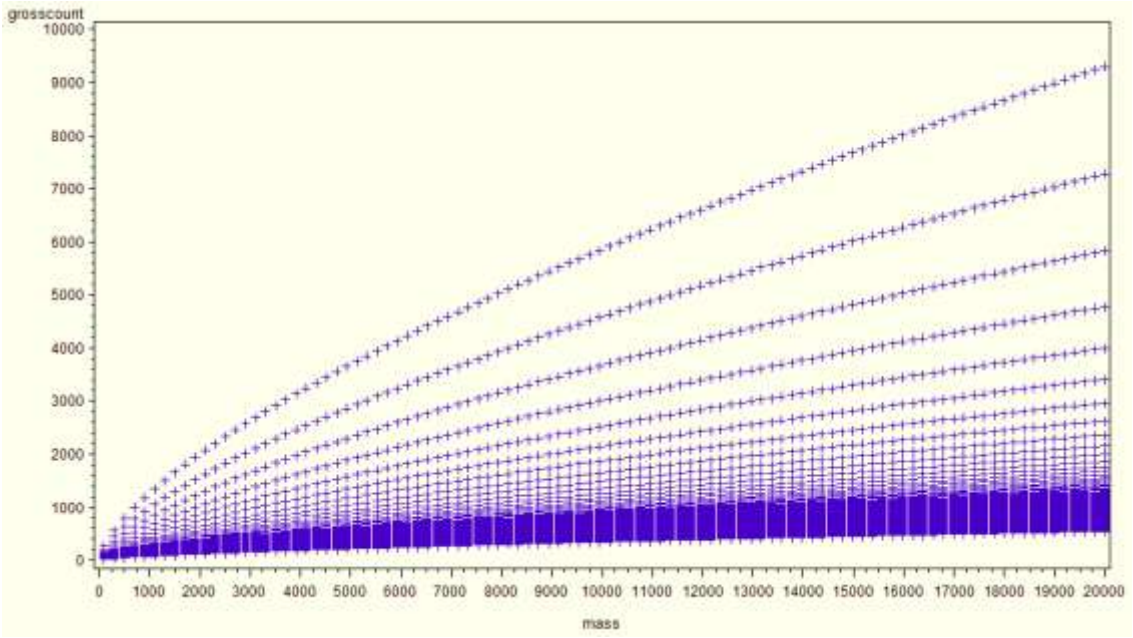

Figure 4.3: Scatter plot of *grosscount* versus *mass* for HEU isotopes

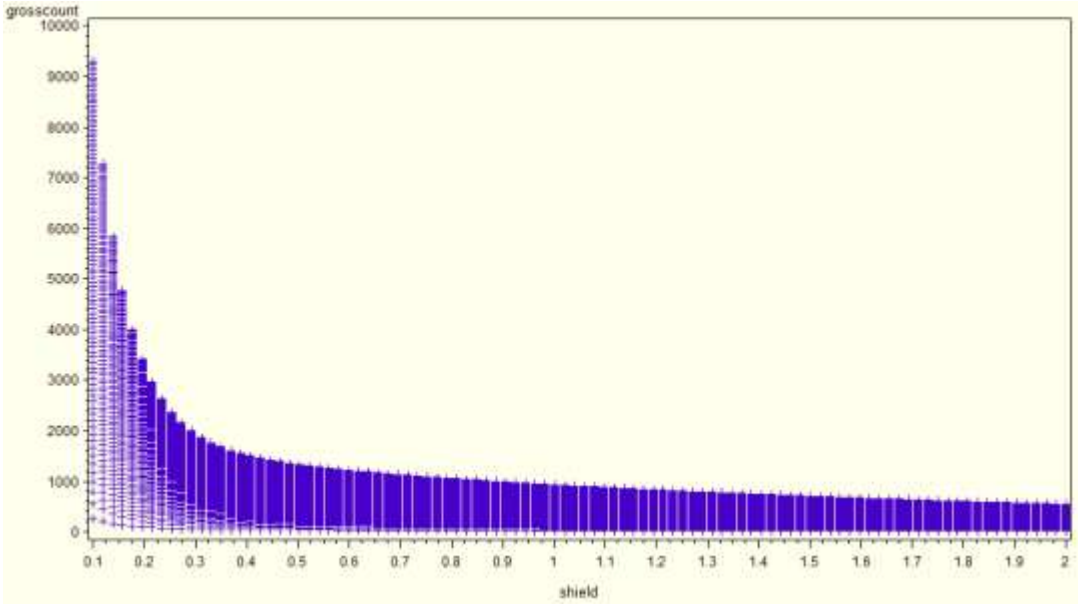

Figure 4.4: Scatter plot of *grosscount* versus *shield* for HEU isotopes

Table 4.15: Curvilinear Regression Output for Plutonium Isotopes

Source	DF	Sum of Squares	Mean Square	F Value	Pr > F
Model	2	48919.55809	24459.77904	182127	<.0001
Error	9997	1342.60643	0.1343		
Corrected Total	9999	50262.16452			

R-Square	Coeff Var	Root MSE	ln_grosscount Mean
0.973288	5.632234	0.366471	6.506671

Source	DF	Type I SS	Mean Square	F Value	Pr > F
ln_mass	1	3383.52276	3383.52276	25193.6	<.0001
shield	1	45536.03533	45536.03533	339060	<.0001

Source	DF	Type III SS	Mean Square	F Value	Pr > F
ln_mass	1	3383.52276	3383.52276	25193.6	<.0001
shield	1	45536.03533	45536.03533	339060	<.0001

Parameter	Estimate	Standard Error	t Value	Pr > |t|
Intercept	5.1438	0.0334331	153.85	<.0001
ln_mass	0.6667	0.00420014	158.72	<.0001
shield	-1.4936	0.00256502	-582.29	<.0001

Table 4.16: Curvilinear Regression Output for HEU Isotopes

Source	DF	Sum of Squares	Mean Square	F Value	Pr > F
Model	2	6731.767433	3365.883716	46409	<.0001
Error	9997	725.048122	0.072527		
Corrected Total	9999	7456.815555			

R-Square	Coeff Var	Root MSE	ln_grosscount Mean
0.902767	4.289688	0.269308	6.278022

Source	DF	Type I SS	Mean Square	F Value	Pr > F
ln_mass	1	4269.230799	4269.230799	58864.4	<.0001
shield	1	2462.536634	2462.536634	33953.6	<.0001

Source	DF	Type III SS	Mean Square	F Value	Pr > F
ln_mass	1	4269.230799	4269.230799	58864.4	<.0001
shield	1	2462.536634	2462.536634	33953.6	<.0001

Parameter	Estimate	Standard Error	t Value	Pr > |t|
Intercept	1.2773	0.02515862	50.77	<.0001
ln_mass	0.6667	0.00274778	242.62	<.0001
shield	-0.8957	0.00486119	-184.26	<.0001

5 CONCLUSIONS AND FUTURE RESEARCH

This report investigates the application of PVT-based RPM systems for detecting smuggled nuclear materials. To address the problem of the inefficiency of current detection technology discriminating NORM from SNM while greatly increasing operational cost and decreasing operational sensitivity, it is critical to develop a new effective detection strategy. For this purpose, we are focusing on characterizing the spectral signatures of different radioactive materials to help better predict detection probabilities for RPMs.

By utilizing a variety of statistical regression models, we have successfully analyzed the impact of several important factors on system response. For the situation of having a single predictor (mass of nuclear isotope), we show that the mass of different isotopes play a distinct role in the resulting radiation spectra when energy windowing technique is applied. For the situation of having two system predictors (total mass of isotopes and thickness of shielding material), we find that the regression is not achievable based on separate energy windows, but is well accomplished on the evaluation of the whole range of spectrum. A nonlinear relationship between gross count of gamma photons and the two predictors is achieved by curvilinear regression analysis and justified by the behavior of the system's physics.

Although we have examined the system behavior under the above circumstances, we have not yet investigated the effect of other factors on the system response, such as the intensity of natural background radiation, the position of threat sources in cargo,

cargo type for each individual isotope, and so forth. These are all significant factors that could make the prediction of detection probabilities difficult to achieve, and need to be further studied in the future.

References

[1]Ely, J.H., R.T. Kouzes, J.E. Schweppe, E. Siciliano, D. Strachan, D. Weier. 2006. The use of energy windowing to discriminate SNM from NORM in radiation portal monitors. *Nuclear Instruments and Methods in Physics Research A* 560, 373-387.

[2]Geelhood, B.D., J.H. Ely, R. Hansen, R.T. Kouzes, J.E. Schweppe, R.A. Warner. 2003. Overview of portal monitoring at border crossings. Nuclear Science Symposium Conference Record, Portland, OR.

[3]Kouzes, R.T., J.H. Ely, B.D. Geelhood, R. Hansen, E. Lepel, J.E. Schweppe, E.R. Siciliano, D. Strom, R.A. Warner. 2003. Naturally occurring radioactive materials and medical isotopes at border crossings. Nuclear Science Symposium Conference Record, Portland, OR.

[4]Thoreson, G.G., E.A. Schneider. 2010. Efficient Calculation of Detection Probabilities. *Nuclear Instruments and Methods in Physics Research A, in press.*

[5]Agresti, A. 1990. *Categorical Data Analysis*. Wiley Series in Probability and Mathematical Statistics, New York.

[6]Hosmer, D.W., S. Lameshow. 1989. *Applied Logistic Regression*. Wiley Series in Probability and Mathematical Statistics, New York.

[7]So, Y., W.F. Kuhfeld. Multinomial logit models. SAS Institute Inc., SAS Technical Report TS-722G, Cary, NC.

[8]Derr, R.E. Performing exact logistic regression with the SAS System. SAS Institute Inc., SAS Technical Report P254-25, Cary, NC.

[9]SAS Institute Inc., SAS/STAT User's Guide, Cary, NC.

[10]SAS Institute Inc., SAS Procedures Guide, Cary, NC.

[11]DeMaris, A. 1995. A tutorial in logistic regression. *Journal of Marriage and the Family* 57, 956-968.

[12]Peng, C.J., K.L. Lee, G.M. Ingersoll. 2002. An introduction to logistic regression analysis and reporting. *The Journal of Educational Research* 96, 3-14.

[13]Fox, J., R. Anderson. 2006. Effect displays for multinomial and proportional-odds logit models. *Sociological Methodology* 36, 225-255.

[14]Tse, Y.K. 1987. A diagnostic test for the multinomial logit model. *Journal of Business & Economic Statistics* 5, 283-286.

[15]Hu, S., C. Li, C. Lee. 2010. Investigation of key factors for accident severity at railroad grade crossings by using a logit model. *Safety Science* 48, 186-194.

[16]Lee, J. 1992. Cumulative logit modeling for ordinal response variables – applications to biomedical-research. *Computer Application in the Biosciences* 8, 555-562.

[17]Winship, S., R.D. Mare. 1984. Regression models with ordinal variables. *American Sociological Review* 49, 512-525.

[18]Peterson, B., F.E. Harrell. 1990. Partial proportional odds models for ordinal response variables. *Journal of the Royal Statistical Society. Series C* 39, 205-217.

[19]Fader, P.S., J.M. Lattin, J.D.C. Little. 1992. Estimating nonlinear parameters in the multinomial logit model. *Marking Science* 11, 372-385.

[20]Guadagni, P.M., J.D.C. Little. 1983. A logit model of brand choice calibrated on scanner data. *Marketing Science* 2, 203-238.

[21]Amedeo, D.L. 2006. A logit model with a variable response and predictors on an ordinal scale to measure customer satisfaction. *Quality & Reliability Engineering International* 22, 591-602.

[22]Agresti, A., J.B. Lang. 1993. A proportional odds model with subject-specific effects for repeated order categorical responses. Biometrika 80, 527-534.

Vita

Fei Tong was born in Hefei, P.R. China, on December 16, 1986. She received her Bachelor of Science degree in Mechanical Engineering from Tianjin University in China in 2007. She entered The University of Texas at Austin in September 2008, where she continued her graduate study in Operations Research and Industrial Engineering.

Permanent address: 3431 N Hills Dr Apt 321, Austin, TX 78731

This report was typed by the author.